Upconversion Luminescence Sandwich Assay For Detection of Influenza H7 Subtype

Ming-Kiu Tsang, Yuen-Ting Wong, Tik-Hung Tsoi, Wing-Tak Wong and Jianhua Hao**

Dr. M.-K. Tsang, Y.-T. Wong, Prof. J. Hao
Department of Applied Physics,
The Hong Kong Polytechnic University,
Hung Hom, Hong Kong, P. R. China
E-mail: jh.hao@polyu.edu.hk

Dr. T.-H. Tsoi, Prof. W.-T. Wong
Department of Applied Chemistry and Biology,
The Hong Kong Polytechnic University,
Hung Hom, Hong Kong, P. R. China
E-mail: w.t.wong@polyu.edu.hk

Keywords: upconversion nanoparticles, biodetections, gold nanoparticles, DNA oligonucleotides, bionanotechnologies

With large anti-Stokes shifts and background-free signals, upconversion luminescent (UCL) screening assays have been a promising method to reduce the transmission of influenza epidemic, which can critically alleviate the disease burden and extra annual deaths. In this work, a luminescent resonance energy transfer sandwich assay is developed, which utilizes core-shell upconversion nanoparticles and gold nanoparticles as the donor and acceptor, respectively. The influenza H7 gene of H7N9 virus is used as the target for optimization of the assay. Importantly, the hybridization time of the assay is approximately (app.) 40 min and the specificity test indicates the probes are specific towards the H7 target. The limit of detection of the system is app. 134 picomolar (app. 3.22 x 10^{10} molecules). Moreover, the assay is tested with the use of polymerase chain reaction validated samples from human isolates. The results are promising for implanting future on-site rapid influenza screening application.

1. Introduction

Influenza (flu) has been threatening the world for decades and caused substantial number of death yearly.[1] The flu viruses also mutate to infect human beings by antigenic shift. As a result, it is urgent to explore versatile detection schemes for probing and visualizing the presence of the viruses. The conventional enzyme-linked immunosorbent assay (ELISA) and real-time polymerase chain reactions (qPCR) are well-recognized tools for the detection of flu viruses by either detecting the antigens or oligonucleotides (oligos) of the viruses.[2–5] Considering the increasing demand and development, an ideal screening platform should be capable of performing simple, rapid and specific readout. Therefore, the new technology can rapidly screen the potential patients with short turnover time. Electrochemical sensors detect the presence of influenza virus genes by voltammetric, impedemetric or chronoamperometric approaches.[6] Those sensors increase the limits of detection (LOD) by using signal amplifiers but the hybridization times are usually long.[7] On the other hand, colorimetric sensor produce visible color changes upon the presence of the virus genes. The simplicity in design and readout of these sensors had attracted substantial attention. Gold nanoparticles (AuNPs) are one of the promising candidates for such detection strategy because of their high extinction coefficient and aggregation-dependent color change.[8,9] Despite the advantages, AuNPs are surface-sensitive and may induce undesired aggregations due to high ionic strength and concentration of ions, resulting in false-positive signals.

Apart from those approaches, optical detection has drawn substantial attention because of their simplicity, sensitiveness and multiplexity.[10,11] It is the fact that organic dyes are widely used in conventional qPCR assays via downconversion processes.[4,12,13] However, the dyes demonstrate undesirable emissive properties such as poor photostability, broad emission band

and small Stokes shift.[14] Therefore, they were usually employed as quenchers in nanoparticle-based detection systems.[15 17] High energy excited quantum dots (QDs) are another representative fluorophores in downconverting assays.[18 20] The excitation may induce background fluorescence and broad emission peaks, contributing to severe cross-talking problem. To address these limitations, near-infrared (NIR) triggered upconversion luminescence (UCL) in lanthanide-doped upconversion nanoparticles (UCNPs) is very promising in bio-detection. They not only display large anti-Stokes shift[21,22] but also poses minimal damage to the gene oligos. In addition, the long-lived UCL signal is easily distinguished from the short-lived background signal. As a result, UCNPs were used to detect different oligos and analytes. [23 28] The assays involved highly distance-dependent luminescence resonance energy transfer (LRET) between energy donor and acceptor, in which the luminescent intensity changes with the separation between the energy pair.[29] In this work, green emitting UCNPs and AuNPs are selected as the LRET pair owing to their well-matched emission and extinction spectrum, while AuNPs exhibit excellent extinction coefficient and photo-stability. The size of the nanoparticles played important roles in hybridization[30] because AuNPs demonstrate size-dependent absorption property and it can alter the stability of the hybridized DNA duplex. In addition, the size ratios of the UCNPs and AuNPs affect the formation of UCNPs-AuNPs hybrid structures. Taking advantages of 808 nm excitation of Nd^{3+} ions that can minimize heat-induced dehybridization or oligo damages while improving upconversion efficiency in aqueous environment, core-shell $NaGdF_4$:Yb/Er@$NaGdF_4$:Yb/Nd UCNPs (csUCNPs) were adopted as the energy donor for sandwich detection. In the detection scheme, the oligo probes were efficiently immobilized onto the csUCNPs and AuNPs by carbodiimide crosslinking and acid-assisted chemisorption, respectively. Upon the presence of target oligos, these nanoparticles are brought into close intimacy and enables LRET to occur associated with UCL changes. The small-sized AuNPs are suitable for effective oligo hybridization at app. 40 min. In addition, the PCR-validated

H7N9 human isolates of influenza A virus were tested to reveal the potential of the biosensor towards clinical applications.

2. Results and discussion

2.1. Structure and physical properties

The $NaGdF_4$:Yb/Er@$NaGdF_4$:Yb/Nd csUCNPs were synthesized by a previously reported coprecipitation method.[31] **Figure 1**(a) and (b) show the TEM image of the oleate capped csUCNPs and csUCNPs-probe, respectively. It should be noted that a non-crystalline layer appears after the probe conjugation. Moreover, the selected area electron diffraction (SAED) pattern in **Figure S1**(a) confirms the hexagonal phase nature of the as-prepared csUCNPs. Apart from the csUCNPs, the citrate-stabilized AuNPs are responsible for attaining high quenching efficiency of the detection system. The AuNPs were synthesized by a step by step seed growth synthetic protocol.[32] The size of the AuNPs can be precisely controlled by sequential shots of $HAuCl_4$ precursors. Also, the size is crucial for manifesting the spatial condition for initial contact, zipping and stability during hybridization. **Figure S1**(b) and **Figure 1**(c) present the morphology of the as-synthesized AuNPs and AuNPs-probe, respectively. The instantaneous oligo probe modification does not induce aggregation in the hybridization buffer and the immobilized oligo ensures good dispersity. Then, the csUCNPs-probe is surrounded by the AuNPs-probe after oligo hybridization, forming a network structure (**Figure 1**(d)).

2.2. Optical and surface characterization

The surface of the NPs should be heavily functionalized to ensure high stability and high rate of hybridization in the buffer medium.[30,33] The oleate layers of the as-synthesized csUCNPs

were removed by hydrochloric acid for hydrophilicity as ligand-free csUCNPs.[34] Then, polyacrylic acid (PAA)-modified csUCNPs were prepared for bioconjugations of the oligo probe via coordination interactions between carboxylic groups and lanthanide ions. Subsequently, the oligo probe was conjugated onto the carboxylic acid terminals via carbodiimide/N-hydroxysuccinimide (EDC/NHS) covalent crosslinking reaction (**Figure 2**).

Figure S2(a) presents Fourier transform infrared (FTIR) spectra of the oleate and PAA-csUCNPs. The disappearance of the two major peaks at 2928 and 2851 cm^{-1} indicated the successful removal of the $-CH_2$ groups in the oleate layer. After PAA modification, a large and broad absorption peak was observed at 3446 cm^{-1}.[35] In addition to the PAA-csUCNPs, the vast amount of citrate groups on the AuNPs contributes to the highly negative zeta potentia □ va ue [24] After the instantaneous probe conjugation, the AuNPs-probe displays a ess negative □ va ue due to the phosphate backbone of the oligo probe. Importantly, the distribution of the □ remains narrow as shown in **Figure S2**(b). The conjugation efficiencies of the oligo probes play an important role in the hybridization rate; therefore UV-vis spectroscopy was performed to study the conjugation efficiency. **Figure S3**(a) and (b) show the calibration line for the thiolated-probe with FAM molecule (P1-FAM). After that, excess DTT was used to displace the conjugated P1-FAM and the luminescent intensity at 520 nm was used as the reporting signal for quantifying the conjugated probe on AuNPs. It was found that 63 % of probe conjugated onto the AuNPs. Apart from UV-vis technique, inductive couple plasma-optical emission spectroscopy (ICP-OES) was performed to estimate the amount of AuNPs-P1 after conjugation. **Table S1** suggests that the 47 % of the AuNPs-P1 can be recovered by centrifugation. In addition to AuNPs-P1, the absorption spectrum of the P2-Cy3 and csUCNPs-P2-Cy3 **(Figure S4)** were compared to estimate the conjugation efficiency of the EDC/NHS reaction. By monitoring the absorption maxima at 550 nm, it was found that 45 % of the probe was conjugated onto the csUCNPs. Apart from surface, the

optical properties of the nanoprobes are equally important because LRET requires spectral overlapping of the energy donor and acceptor. **Figure S5**(a) shows the upconversion emission spectra of the PAA-csUCNPs and csUCNPs-probe. The emission increased reasonably after oligo conjugation because the oligo layer shielded the csUCNPs from the hydroxyl oscillators in the buffer medium. Moreover, the absorption spectra of the AuNPs are presented in **Figure S5**(b). The maxima and width of the AuNPs-probe did not show significant change after probe oligo modification, which indicates the high quality and efficiency of the modification. Importantly, the emission and absorption spectra of csUCNPs-probe and AuNPs-probe overlap well for LRET upon hybridization.

2.3. Detection scheme

The homogeneous sandwich detection scheme (**Figure 3**) utilizes oligo-modified csUCNPs and AuNPs as probe for capturing the subtype target genes. The sequences of the oligos were summarized in **Table 1**. The probe oligo genes were designed according to the World Health Organization (WHO) protocol for diagnosis of human influenza viruses.[36] Moreover, the oligo probes were tethered with poly-A bases (Underlined) for effective probe conjugation to the nanoparticles and hybridization.[37,38] The number of tethering on the amine-modified oligo and the thiolated oligo is 10 and 8 of bases, respectively. The amine probe oligo was conjugated on the polyacrylic acid modified csUCNPs via EDC/NHS covalent crosslinking reaction while the thiol-probe oligo was immobilized on the AuNPs with the assistance of acid and salt. The 808 nm laser excitation does not pose any heating effect to the assay, which may disturb the stability of the hybridized structures. Then, LRET occurs as a result of oligo duplex formation during hybridization. The green emission from csUCNPs is absorbed by the AuNPs; therefore the decrement is used to quantify the amount of virus oligo.

2.4. Sandwich homogeneous assay

It is essential to find out the melting characteristics of the assay because this determines the temperature for hybridization condition. **Figure 4**(a) shows the melting curve from 45 to 70 ^{o}C with 10 nM of H7 target monitored at 260 nm. The T_m value corresponded to the half of the percentage drop in the absorption at 260 nm (A_{260}), which was app. 56 ^{o}C. The nanoprobes were dispersed in molecular biology grade water with Tris-HCl (pH 7.6) prior to hybridization. Then, the probes were incubated at 90 ^{o}C to destroy all local entanglements and secondary structures, followed by 55 ^{o}C incubation. The hybridization stage was maintained for 40 min in the heat block. After cooling to room temperature, the upconversion emission spectra of the samples were measured by using 808 nm diode laser. **Figure 4**(b) shows the upconversion spectra of the stimulated H7 subtype detections using the sandwich assay. The control (named reabsorption in the spectra) sample consisted of the csUCNPs-P1 and AuNP-P2 to eliminate the intensity drops due to simple reabsorption. The emission intensities at 540 nm decreased with increasing amount of H7 targets. The observation was attributed to the increased LRET between csUCNPs-P2 and AuNPs-P1. The lowest detectable concentration was app. 100 picomolar (pM) and the quenching efficiency (QE) saturated at app. 10 nM target. A linear response (**Figure 4**(c)) was found at 100 pM to 1 nM as $y = 27.2x + 15.4$. Moreover, the limit of detection (LOD) was estimated at 134 pM with an equivalent amount of H7 3.22 x 10^{10} molecules. The detection was repeated for five times and the LOD was calculated by three times the standard error in response divided by the slope of the linear fitting.[39] Moreover, the LOD of the current assay was compared with the other reported sensors in **Table 2**. It is comparable to the LOD of luminescent/fluorescent-based homogeneous assays, which was in femtomolar (fmol) range. Furthermore, the emission lifetime at 540 nm of reabsorption was compared with that of 1 nM H7 target **(Figure 4**(d)). The lifetime indicated a shift of 30.4 %, because the LRET process provides extra pathway for the decay.

2.4. Specificity

Specificity is a paramount specification of the assay because the family of influenza A consists of many subtypes. Therefore, the specificity of the assay (**Figure 5**) was evaluated with 1 nM concentration of H7, N9 and 3 BM target samples. The H7 target oligo showed a quenching efficiency at app. 67 %, which was in good agreement with the previous results.[23,24] Owing to the three base mismatches, the initial contact process was not efficient, hence yielding app. 20 % quenching. As H7N9 is a popular avian influenza in Hong Kong, its N9 counterpart was selected for the specificity test. The results suggested that the H7 probes can differentiate clearly between H7 and N9 gene.

2.5. Detection of PCR-validated sample

A useful and practical assay should be primarily tested with human isolate samples to explore their potential for future applications. The PCR samples of H7 gene were validated according to the WHO protocol for diagnosis of human influenza viruses. **Figure 6**(a) shows the gel photography of the sample processed after PCR that consists of 12 lanes. Three cDNAs of human isolate was added individually as follows: lane 1, 5 and 9 (H7N9); lane 2, 6 and 10 (H1N1) and lane 3, 7 and 11 (H5N1). H7 (lane 1-4), H1 (lane 5-8) and H5 (lane 9-12) specific HA primers were used to verify the specificity of primers. Lane 4, 8 and 12 are the negative controls for each HA gene, correspondingly. The results indicate that the specific H7 gene was amplified by PCR. **Figure 6**(b) presents the emission spectra of the sample at 10 nM and 100 pM. The inset shows the gel electrophoresis results for validating the correct H7 gene. The minimum and maximum QE was app. 14.3 and 30 %, respectively (**Figure 6**(c)). The QE was not as high as the results in the simulated sample detection experiment. The reduced QE may be attributed to the presence of some non-specific targets, such as polymerases, primers, ions and residual deoxyribonucleotide triphosphates. The Au-probe tends to disperse in the medium rather than forming network structure with the csUCNP-probe (**Figure 6**(d)). This

was due to the absence of complementary H7 target for forming network structure for LRET. As a result, the csUCNP-probe also tends to pack closely together. Moreover, the lifetime measurement for the control sample and the 10 nM H7 PCR-validated sample was carried out to support the LRET phenomena (**Figure 6**(e)). The prolonged lifetime of the 10 nM H7 PCR-validated sample justified the LRET between csUCNP-probe and Au-probe. Nevertheless, the results revealed the potential of the developed UCL-sandwich assay for screening of clinical samples.

3. Conclusions

We have developed a sandwich assay based on $NaGdF_4$:Yb/Er@$NaGdF_4$:Yb/Nd csUCNPs and citrated-stabilized AuNPs. The NPs were heavily functionalized with target specific oligo probes to achieve rapid and specific detection. The 808 nm laser excitation avoids thermal agitation that may disturb the oligo duplex and background fluorescence. The assay was firstly tested with simulated H7 gene target and a linear response was found in the range from 100 pM to 1 nM. The LOD of the assay was app. 134 pM (3.22×10^{10} molecules) with clear differentiation from its N9 gene counterpart. Moreover, we step forward to test the assay with PCR-validated samples. The detection results suggested the assay was able to detect the H7 gene target and it had great potential for future virus gene screening applications.

4. Experimental Section

4.1. Synthesis of core-shell $NaGdF_4$:Yb/Er@$NaGdF_4$:Yb/Nd csUCNPs

Synthesis of $NaGdF_4$:Yb/Er core UCNPs

In typical coprecipitation synthesis,[31] Ln^{3+} acetate (Ln^{3+} = Gd^{3+}, Yb^{3+} and Er^{3+}, 0.4 mmol) with designated molar ratio were added to a 50 mL three-necked flask. After that, OA (4 mL) and ODE (6 mL) were added to the same flask under magnetic stirring. The mixture was heated to 150 °C for 1 h. The heating mantle was removed and the mixture was allowed to cool down to room temperature. Then, NaOH/methanol (1 mmol) and NH_4F/methanol (1.32 mmol) were mixed well and immediately injected into the reaction mixture. After that, the temperature was held at 50 °C for 1 h under vigorous stirring. The flask was degassed in vacuum for 10 min, followed by heating to 290 °C in 1.5 h under argon gas protection. After cooling to room temperature, the crude UCNPs were collected by centrifugation and purified by using cyclohexane and ethanol. Finally, the core UCNPs were dispersed in cyclohexane for further modifications.

Synthesis of $NaGdF_4$:Yb/Er@$NaGdF_4$:Yb/Nd core-shell UCNPs

Ln^{3+} acetate (Ln^{3+} = Gd^{3+}, Yb^{3+} and Nd^{3+}, 0.4 mmol) with designated molar ratio were added to a 50 mL three-necked flask. After that, OA (4 mL) and ODE (6 mL) were added to the same flask under magnetic stirring. The mixture was heated to 150 °C for 1 h. The heating mantle was removed and the mixture was allowed to cool down to room temperature. Then, the as-prepared core UCNPs were injected into the Ln^{3+} precursors under vigorous magnetic stirring. NaOH/methanol (1 mmol) and NH_4F/methanol (1.32 mmol) were mixed well and immediately injected into the reaction mixture. After that, the temperature was held at 50 °C for 1 h. The flask was degassed in vacuum for 10 min, followed by heating to 290 °C in 1.5 h under argon gas protection. After cooling to room temperature, the crude csUCNPs were collected by centrifugation and purified by using cyclohexane and ethanol. Finally, the csUCNPs were dispersed in cyclohexane for further modifications.

4.2. Synthesis of citrate-stabilized gold nanoparticles (AuNPs)

The citrate-stabilized AuNPs were synthesized according to previous report.[32] Briefly, tannic acid (6.67 μL, 2.5 mM), potassium carbonate (66.7 μL, 150 mM) were added to sodium citrate solution (10 mL, 2.2 mM) under vigorous stirring. The mixture was heated to 70 °C with tetrachloroauric acid (66.7 μL, 25 mM) for 5 min. Then, two shots of tetrachloroauric acid (33.3 μL, 25 mM) were added to the medium for every 10 min. After that, the citrate-stabilized AuNPs were stored at 4 °C for further modifications.

Supporting Information

Supporting Information is available from the Wiley Online Library or from the author.

Acknowledgements

The authors would like to acknowledge Ms. Siu-Ying Lau and Prof. Honglin Chen from the State-Key Laboratory for Emerging Infectious Diseases and Department of Microbiology, Li Ka Shing Faculty of Medicine in the University of Hong Kong, for providing PCR validated H7 human isolate samples. This work is financially supported by the Hong Kong Research Grants Council (PolyU 153012/15P) and Area of Excellence Grants (1-ZVGG) of Hong Kong Polytechnic University.

Received: ((will be filled in by the editorial staff))
Revised: ((will be filled in by the editorial staff))
Published online: ((will be filled in by the editorial staff))

References

[1] S.Yamayoshi, Y.Kawaoka, *Nat. Med.* **2019**, *25*, 212.

[2] M.Liu, H.Chen, J.Zhou, Y.Sun, L.Chen, F.Ruan, K.Qin, *J. Med. Virol.* **2019**, 10.

[3] W.Chae, P.Kim, B. J.Hwang, B. L.Seong, *Vaccine* **2019**, *37*, 1457.

[4] G.Boivin, S.Côté, P.Déry, G.DeSerres, M. G.Bergeron, *J. Clin. Microbiol.* **2004**, *42*, 45.

[5] H .Jifincova, T .Jifinec, L Cernikova, A Nagy, M Hav ickova, *Sci. Rep.* **2019**, *9*, 1.

[6] S.Campuzano, P.Yáñez-Sedeño, J. M.Pingarrón, *ChemElectroChem* **2017**, *4*, 753.

[7] I. H.Cho, J.Lee, J.Kim, M. S.Kang, J. K.Paik, S.Ku, H. M.Cho, J.Irudayaraj, D. H.Kim, *Sensors* **2018**, *18*, 1.

[8] A.Sánchez-Iglesias, N.Claes, D. M.Solís, J. M.Taboada, S.Bals, L. M.Liz-Marzán, M.Grzelczak, *Angew. Chemie - Int. Ed.* **2018**, *57*, 3183.

[9] Y. S.Borghei, M.Hosseini, M.Dadmehr, S.Hosseinkhani, M. R.Ganjali, R.Sheikhnejad, *Anal. Chim. Acta* **2016**, *904*, 92.

[10] M.-K.Tsang, G.Bai, J.Hao, *Chem. Soc. Rev.* **2015**, *44*, 1585.

[11] J.Yao, M.Yang, Y.Duan, *Chem. Rev.* **2014**, *114*, 6130.

[12] P.Jiang, D.Kargbo, S.Jalloh, M.Fonnie, V.Sinnah, I.French, aKovoma, F.Kanneh, S.Saffa, J. L. B.Massally, et al., *N. Engl. J. Med.* **2014**, *371*, 2092.

[13] T.Chailangkarn, C. A.Trujillo, B. C.Freitas, B.Hrvoj-Mihic, R. H.Herai, D. X.Yu, T. T.Brown, M. C.Marchetto, C.Bardy, L.McHenry, et al., *Nature* **2016**, *536*, 338.

[14] U.Resch-Genger, M.Grabolle, S.Cavaliere-Jaricot, R.Nitschke, T.Nann, *Nat. Methods* **2008**, *5*, 763.

[15] H.Guo, N. M.Idris, Y.Zhang, *Langmuir* **2011**, *27*, 2854.

[16] M.Kumar, P.Zhang, *Langmuir* **2009**, *25*, 6024.

[17] Y.Liu, M.Chen, T.Cao, Y.Sun, C.Li, Q.Liu, T.Yang, L.Yao, W.Feng, F.Li, *J. Am. Chem. Soc.* **2013**, *135*, 9869.

[18] I. L.Medintz, H. T.Uyeda, E. R.Goldman, H.Mattoussi, *Nat. Mater.* **2005**, *4*, 435.

[19] J.Guo, C.Mingoes, X.Qiu, K.Susumu, J. R.Deschamps, N.Hildebrandt, I. L.Medintz, *ACS Nano* **2018**, *13*, 505.

[20] G.Annio, T. L.Jennings, O.Tagit, N.Hildebrandt, *Bioconjug. Chem.* **2018**, *29*, 2082.

[21] J.Zhou, Q.Liu, W.Feng, Y.Sun, F.Li, *Chem. Rev.* **2015**, *115*, 395.

[22] S.Gai, C.Li, P.Yang, J.Lin, *Chem. Rev.* **2014**, *114*, 2343.

[23] M.-K.Tsang, W.Ye, G.Wang, J.Li, M.Yang, J.Hao, *ACS Nano* **2016**, *10*, 598.

[24] W. W.Ye, M.-K.Tsang, X.Liu, M.Yang, J.Hao, *Small* **2014**, *10*, 2390.

[25] B.Gu, Q.Zhang, *Adv. Sci.* **2018**, *5*, 1700609.

[26] Y.Liu, D.Tu, W.Zheng, L.Lu, W.You, S.Zhou, P.Huang, R.Li, X.Chen, *Nano Res.* **2018**, *11*, 3164.

[27] D.Zhu, Z. Y.Miao, Y.Hu, X. J.Zhang, *Biosens. Bioelectron.* **2018**, *100*, 475.

[28] X.Liu, X.Li, X.Qin, X.Xie, L.Huang, X.Liu, *Adv. Mater.* **2017**, *29*, 1.

[29] P. R.Selvin, T. M.Rana, J. E.Hearst, *J. Am. Chem. Soc.* **1994**, *116*, 6029.

[30] S. J.Hurst, A. K. R.Lytton-Jean, C. A.Mirkin, *Anal. Chem.* **2006**, *78*, 8313.

[31] F.Wang, R.Deng, X.Liu, *Nat. Protoc.* **2014**, *9*, 1634.

[32] J.Piella, N. G.Bastús, V.Puntes, *Chem. Mater.* **2016**, *28*, 1066.

[33] A. W.Peterson, *Nucleic Acids Res.* **2002**, *29*, 5163.

[34] N.Bogdan, F.Vetrone, G. A.Ozin, J. A.Capobianco, *Nano Lett.* **2011**, *11*, 835.

[35] M.-K.Tsang, C.-F.Chan, K.-L.Wong, J.Hao, *J. Lumin.* **2015**, *157*, 172.

[36] World Health Organization, *WHO Information for Molecular Diagnosis of Influenza Virus*, **2015**.

[37] B.Liu, J.Liu, *Anal. Methods* **2017**, *9*, 2633.

[38] X.Zhang, M. R.Servos, J.Liu, *J. Am. Chem. Soc.* **2012**, *134*, 7266.

[39] A.Shrivastava, V.Gupta, *Chronicles Young Sci.* **2011**, *2*, 21.

[40] J.Shi, C.Chan, Y.Pang, W.Ye, F.Tian, J.Lyu, Y.Zhang, M.Yang, *Biosens. Bioelectron.* **2015**, *67*, 595.

[41] Y. D.Ye, L.Xia, D. D.Xu, X. J.Xing, D. W.Pang, H. W.Tang, *Biosens. Bioelectron.* **2016**, *85*, 837.

[42] B.Wu, Z.Cao, Q.Zhang, G.Wang, *Sensors Actuators, B Chem.* **2018**, *255*, 2853.

[43] M.Huang, H.Li, H.He, X.Zhang, S.Wang, *Anal. Methods* **2016**, *8*, 7413.

[44] P.Teengam, W.Siangproh, A.Tuantranont, T.Vilaivan, O.Chailapakul, C. S.Henry, *Anal. Chem.* **2017**, *89*, 5428.

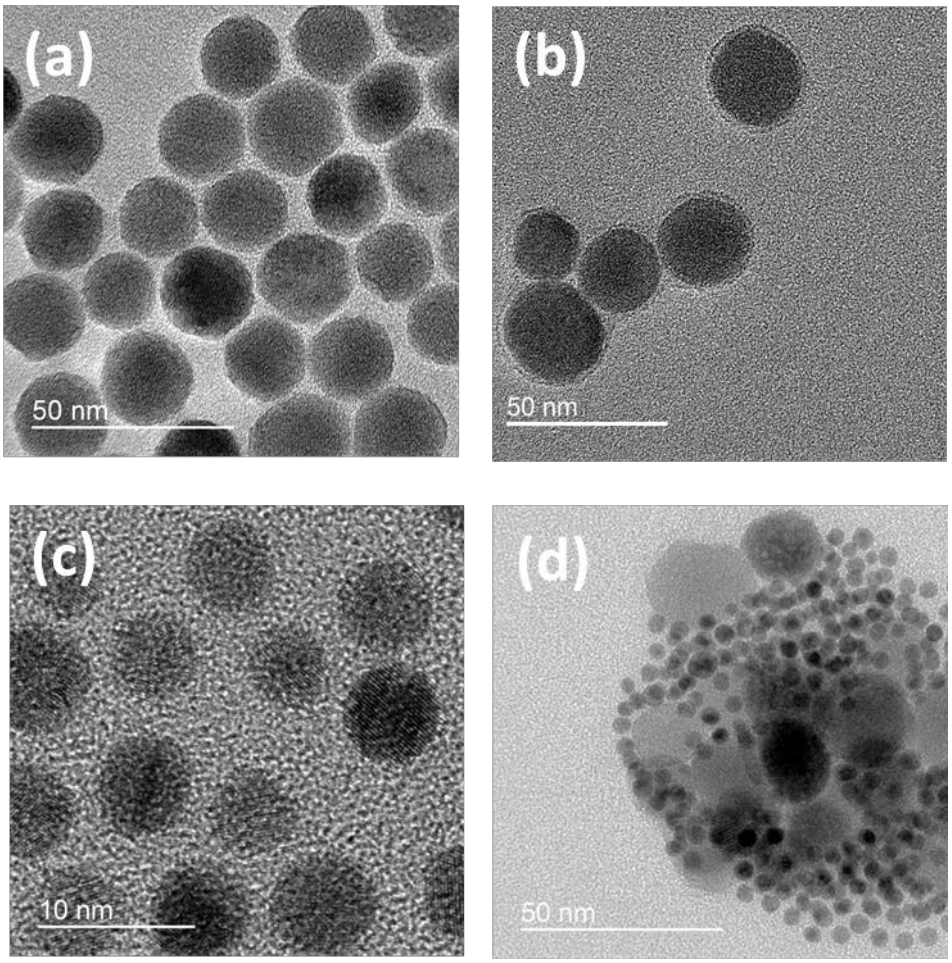

Figure 1 TEM images of (a) OA-csUCNPs, (b) csUCNPs-probe, (c) AuNPs-probe and (d) hybridized duplex structure of csUCNPs-probe and AuNPs-probe.

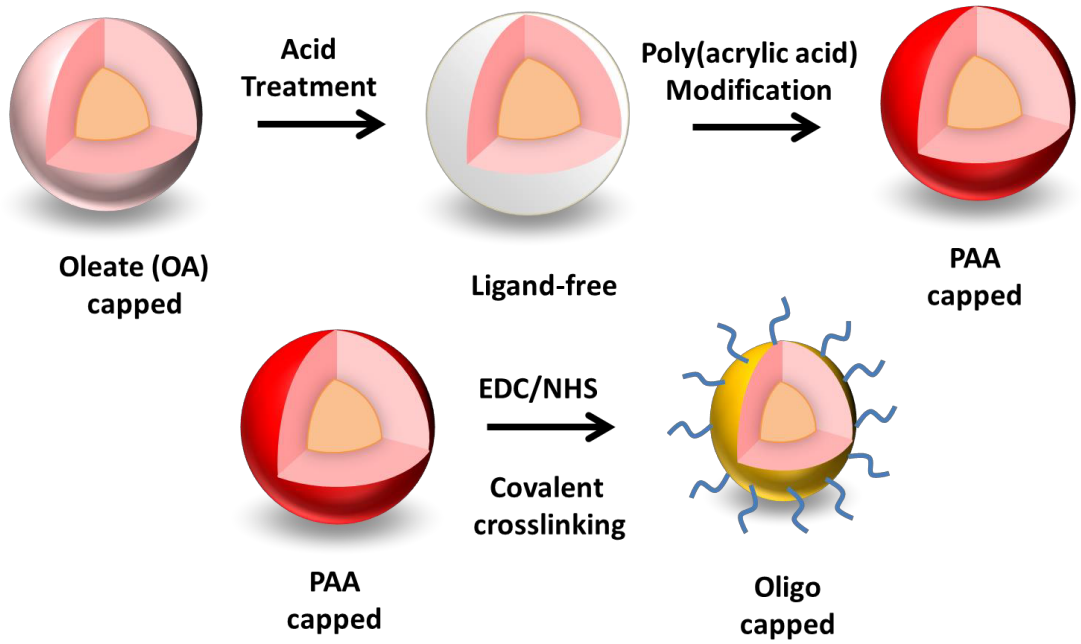

Figure 2 Modification routes of csUCNPs from oleate to probe oligo surface.

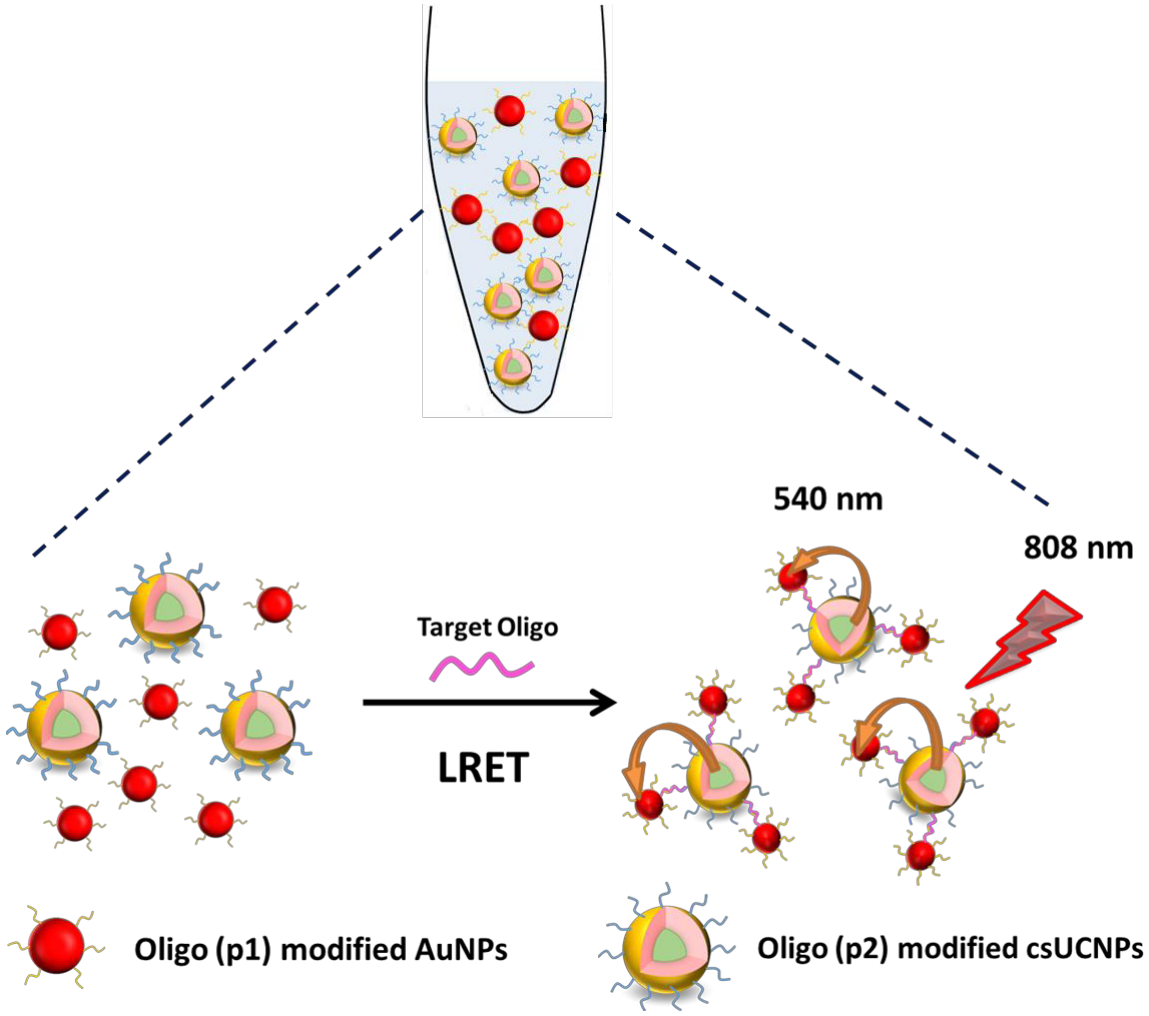

Figure 3 Homogeneous sandwich detection scheme based on Au-P1 and csUCNP-P2.

Table 1 Summary of oligo probe and target sequences. Designs of the probes for hemagglutinin (H7) genes of H7N9 influenza A viruses are according to WHO protocols.[36] The non-complementary bases are represented by bolded text.

Name	Sequence (5'- 3')
P1	SH-AAA AAA AAA ACT AAG CAG CGG
P2	TGA CCC AGT CAA AAA AAA AAA A-NH_2
P1-FAM	SH-AAA AAA AAA ACT AAG CAG CGG -FAM
P2-Cy3	Cy3- TGA CCC AGT CAA AAA AAA AAA A-NH_2
H7 target	CCG CTG CTT AGT TTG ACT GGG TCA
N9 target	GGG TCA TTC GGT CGG GGA TTG TCT
3BM target	CCG C**A**G CTT A**T**T TTG ACT G**A**G TCA

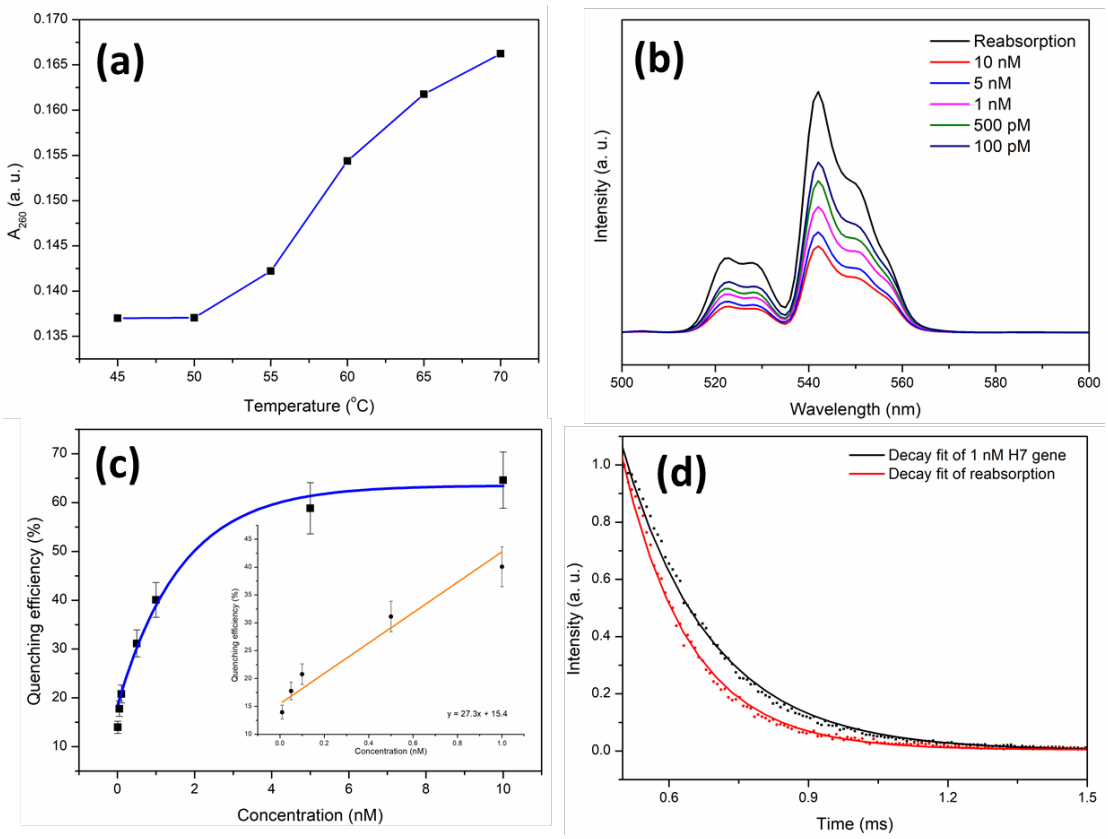

Figure 4 (a) Melting curve of the sandwich assay with H7 target concentration at 10 nM, (b) Upconversion emission spectra of the sandwich assay excited by 808 nm laser, (c) QE of target concentrations from 100 pM to 10 nM (Inset showing the linear response from 100 pM to 1 nM target concentration) and (d) Lifetime measurement of reabsorption and 1 nM H7 target sample.

Table 2 Comparison of LOD in different gene-based detection techniques

Detection method	Linear range	Limit of detection	Ref.
Luminescent	100 pM - 1 nM	67 fmol	This work
Luminescent	Not provided	100 fmol	[40]
Luminescent	1 nM 50 nM	80 fmol	[41]
Luminescent	10 nM 200 nM	6.4 pmol	[42]
Impedemetric	1 nM 1 μM	1.2 pmol	[43]
Colorimetric	20 nM 2500 nM	25 fmol	[44]

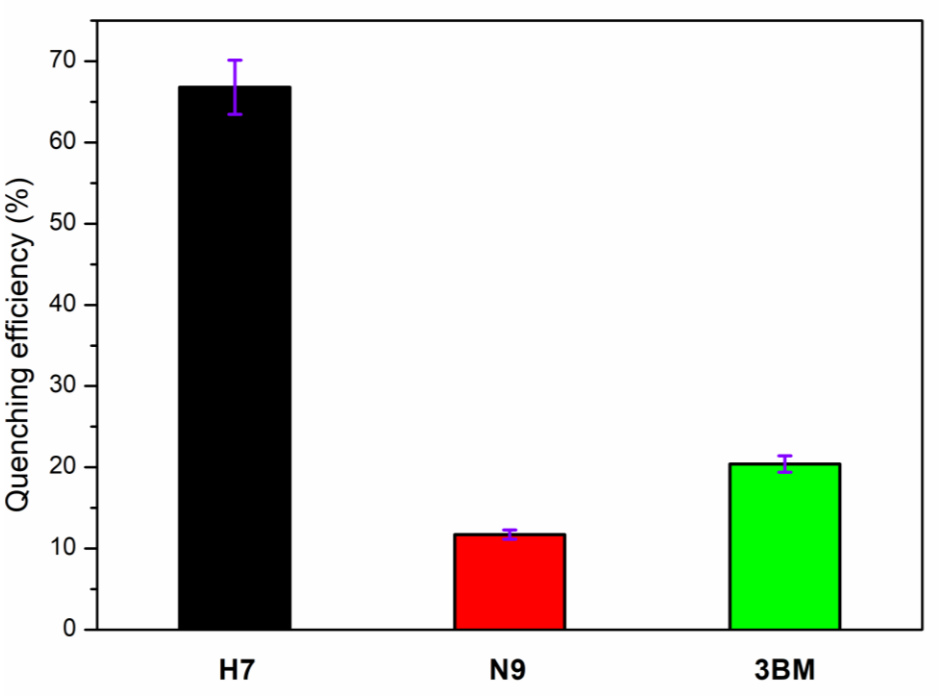

Figure 5 Specificity of the sandwich assay using 1 nM of targets.

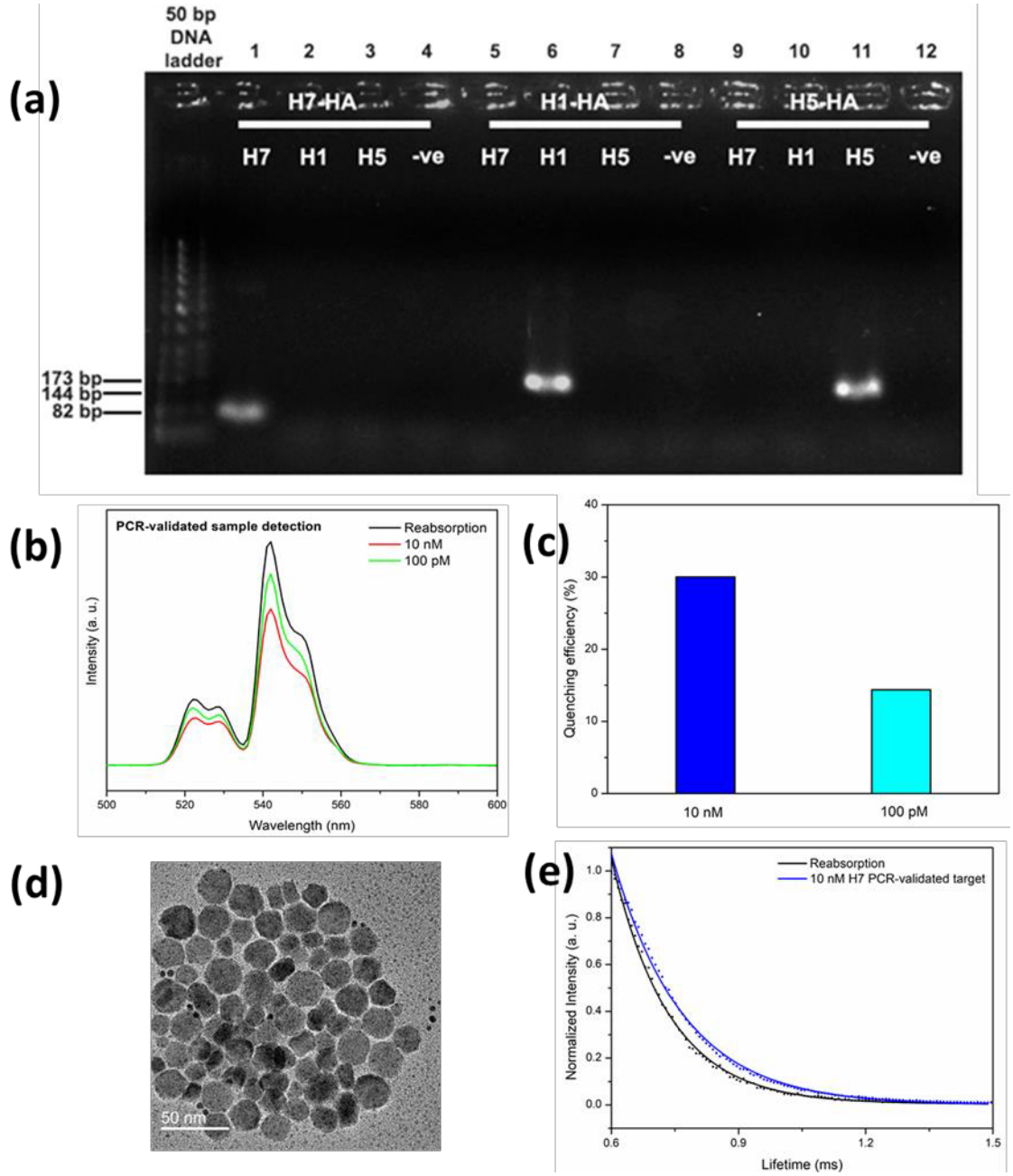

Figure 6 (a) Confirmation of PCR-validated H7 HA sample from H7N9 human isolate by gel electrophoresis of 82 base pairs (bp), (b) Upconversion emission spectra of PCR-validated H7 HA genes (82 base pairs) and (c) QE of 10 nM and 100 pM samples, (d) TEM image of the control sample (csUCNP-probe and AuNP-probe only) and (e) lifetime measurement of the control sample and 10 nM H7 PCR-validated target

The table of contents entry should be 50 60 words long and should be written in the present tense and impersonal style (i.e., avoid we). The text should be different from the abstract text.

Keyword: *Biodetection*

Ming-Kiu Tsang, Yuen-Ting Wong, Tik-Hung Tsoi, Wing-Tak Wong and Jianhua Hao***

Title: *Upconversion Luminescence Sandwich Assay For Detection of Influenza H7 Subtype*

The upconversion luminescent sandwich assay consists of the core-shell upconversion and gold nanoparticles. The nanoparticles were functionalized with oligo probe for H7 influenza subtype detection. The assay shows high specificity and short hybridization time. Moreover, the assay was tested with human isolate samples and the results indicated high potential of the assay for future screening applications.